COBEM 2021 Florianópolis - Brasil
ABCM Associação Brasileira de Engenharia e Ciências Mecânicas
26th ABCM International Congress of Mechanical Engineering
November 22-26, 2021. Florianópolis, SC, Brazil

COBEM-2021-1292
EFFECT OF LASER POWER MODULATION ON POROSITY AND RESIDUAL STRESSES OF SAE 1020 AND 4140 STEEL WELDS

Francisco Cavilha Neto
Laboratory of Precision Engineering—Laser Division (LMP-Laser), Department of Mechanical Engineering, Universidade Federal de Santa Catarina, Santa Catarina, Brazil
franciscocavilha@gmail.com
Milton Pereira
Laboratory of Precision Engineering—Laser Division (LMP-Laser), Department of Mechanical Engineering, Universidade Federal de Santa Catarina, Santa Catarina, Brazil
milton.pereira@ufsc.br
Márcio Celso Fredel
Ceramic & Composite Materials Research Laboratories (CERMAT), Department of Mechanical Engineering, Universidade Federal de Santa Catarina, Santa Catarina, Brazil
m.fredel@ufsc.br
Luis Eduardo dos Santos Paes
Faculty of Mechanical Engineering, Center for Research and Development of Welding Processes (LAPROSOLDA), Federal University of Uberlandia (UFU), Uberlândia, Brazil

Abstract. *The use of a laser with continuous wave (CW) emission as an energy source in welding has revolutionized the industry due to its highly concentrated energy, precision, and versatility. The energy control by the laser through adequate use of hardware and software apparatus has opened up a range of possibilities regarding the beam-piece interaction times and power. In this sense, the present study aims to evaluate the effect of laser power modulation in order to observe the differences and possible improvements from the method in the welding process. The objectives of this work were, mainly, to use different parameters and modulation formats to evaluate some general aspects of the welds such as welding depth, porosity, and residual stresses in two different SAE steels, 1045 and 4140. The pulse frequency was varied to assess, in terms of integrity, the weld morphology as well as the presence of porosity. To analyze the residual stresses through the drilled-hole method combined with speckle interferometry, continuous and modulated welds were produced in SAE 4140 steels plates. The results showed that the power modulation provoked several changes in the morphological characteristics and defects in weld beads produced, reducing porosity and residual stresses.*

Keywords: *Laser welding. Power modulation. Welding defects. Pulse shaping. Residual Stresses. Porosity.*

1. INTRODUCTION

Laser beam welding (LBW) has proven to be better than conventional welding processing since it provides a higher penetration depth and narrow heat-affected zone (HAZ), due to its lower heat input (Santos Paes, 2019; Derakhshan, 2018). However, many defects such as cracks, pores, lack of fusion, and spikes still can be found in the weld and at the vicinities due to the typical heat phenomena present in LBW. These defects can arise due to many reasons mainly because stabilizing the keyhole cavity generation and maintenance, in deep penetration welding, is a difficult task (Zhang, 2018; Kouraytem, 2019; Jiang, 2019). Cracks can occur due to high residual stress close to the yield strength of the base material (Junaid, 2017), which may lead to the need for further post-treatment. Thermal cycles induced by temperature variation during the welding pass cause dilations that are accommodated by the elastoplastic responses of the base material (Lei, 2020; Liang, 2018; Huang, 2016). This results in cyclical internal stress-strain behavior during processing. Tamma *et al.* (2013) reported that local heating of the metal led to heterogenic expansion and yielding may occur since the metal experiences non-uniform contraction and plastic deformation due to fast cooling. In addition, for hardenable materials, the stresses resulting from the solid-state transformation from austenite to martensite have a strong impact on the state of residual stresses (Kim, 2009; Deng, 2006; Paddea, 2012).

With regards to porosity formation, Huang *et al.* (2018) identified that the instability and oscillations of the keyhole were responsible for the trapping of bubbles during the solidification of aluminum and steel alloys, leading to high levels of porosity in the two alloys. The researchers observed that the bubble trapping phenomenon occurred in response to oscillations of the keyhole. Lin *et al.* (2017) showed that porosity formation occurs in three stages: bubble formation, bubbles floating to the back of the molten pool, and bubbles capture by solidification. Porosity can be avoided by preventing one of these steps. The authors' simulation stated that the strong melt flow behind the keyhole is the main reason for pore formation because it leads to keyhole collapse, resulting in significant fluctuations in the keyhole depth

and bubble formation. According to Zhang *et al.* (2019) porosity can be explained as a result of three phenomena: keyhole instability, shielding gas entrapment, and hydrogen segregation. In the first case, the pores produced are generally large and irregular in shape. They are formed by the strong oscillatory cavity movements, which lead to the trapping of gases from the vaporization of base material at the bottom of the keyhole. The pores in the second case are spherical and originate mainly from bubbles formed by shielding gas that enters the cavity, and they are unable to submerge due to the high welding speed, high penetration depth, or rapid keyhole oscillation. Finally, the third case is characterized by spherical micrometric (< 100 μm) pores, originating from hydrogen segregation.

In contrast to conventional welding processing methods, in power modulation, the amount of energy that is transferred to the component can change over time, and this affects the thermal cycles resulting from this interaction. One of the main advantages, along with those previously mentioned, is the possibility of varying the parameters during processing. Several formats can be used, depending on the objective, for instance, square, sinusoidal, pyramidal, or stepped waves. The use of this method can reduce the energy input, the amount of energy per unit of length, and the abrupt power extinction, causing the heat to flow in different amounts during the process. This technique has been used by several researchers in order to reduce welding defects, such as pores (Matsunawa, 1998; Cavilha Neto, 2021) and cracks (Schaefer, 2017), to refine the fusion zone grain size in steels (Cavilha Neto, 2020), and to reach greater depths of penetration using average powers similar to the traditional continuous power regime (Tsukamoto, 2003). Stritt *et al.* (2010) applied laser power modulation to state that not only does the average laser power and focus diameter has a strong influence on penetration but also the amount of energy supplied within a certain time interval, which can be rapidly changed by modulation. Matsunawa *et al.* (1998) reported that pulse overlap in square power modulation acts by remelting the structure formed in the first pulse, releasing pores trapped by rapid solidification, which can be compared with the multi-pass stress relief method. Huang *et al.* (2016) reported that weld distortions were linearly related to the laser power per unit of length and therefore an increase in the welding speed can reduce the occurrence of deformation.

Given the aforementioned works, the benefits arising from the laser power modulation method are clear, which opens up space for further investigation in the search for high-performance components with fewer defects or desirable microstructural characteristics. In this sense, this work aimed to investigate the effect of power modulation on different SAE steels, in order to achieve weld beads with higher penetrations, lower porosity, and residual stresses. Each try of enhancement was isolated to a better understanding of the results. SAE 4140 steel was chosen to observe residual stresses due to the high hardenability. SAE 1020 was chosen to evaluated porosity due to the less complex microstructure.

2. MATERIALS AND METHODS

2.1 Processing Apparatus and Characterization

The experiments were performed using a YLS 10000 fiber laser source (IPG Photonics) with a maximum power of 10 kW. The laser beam parameters were: wavelength of 1070 nm, theoretical spot size diameter of 800 μm, and beam parameter product (BPP) of 8 mm*mrad. The focus was set at a depth of 6 mm from the surface. Argon gas was used as the shielding gas at 10.0 l/min. For each set of parameters, three sample beads were produced to check the repeatability. The beads were replicated to confirm the results.

The standard metallographic procedure was applied to longitudinal and transversal cross-sections. An optical microscope (Olympus BX60m) was used to acquire the macrographs. ImageJ software (Papadopulos, 2007) was employed to obtain the pore area and penetration depth measurements through image analysis and a depth uncertainty range of ± 0.1 mm was assumed. Beads with 40 mm of length were produced using continuous and modulated laser power. In all cases, the same average energy parameter (power to welding speed ratio) was used in order to investigate the influence of modulation.

The residual stress measuring technique used combines the hole drilling method and speckle interferometry (instead of traditional strain gauges) for the identification of the displacements around the hole, to measure the stress states in a specific surface point. The holes were drilled up to a depth of 1 mm to identify the residual stress profile in the shallow layers of the material. The holes were located on the base metal at a distance of 3 mm from the bead center and 10 mm away from the extremities in order to be applied on a flat and representative surface (necessary for the measurement of the displacements around the hole) and localized in a high-stress concentration zone in beads. The method accuracy is explained in works of Viotti *et al.* (2013) and Albertazzi *et al.* (2015).

2.2 Residual Stresses Study Parameters

The average power level was set at 3 kW and welding speed at 0.5 m/min. These values resulted in an energy level of 360 kJ/m and a total welding time of 4.8 seconds per bead. For the continuous wave (CW) mode, the energy was delivered continuously and for the power modulated emission (MW), square (MW1) and step-shaped (MW2) waves were set up with 50 Hz frequency, 6 kW pulse, and 0 kW base power, as shown in Figure 1. All parameters were selected in order to produce beads with partial penetration which is sufficient to test the hypothesis. Moreover, full penetration may produce stresses induced by displacements in the plate and other phenomena depending on more variables such as sample fixation,

which could affect the comparison by mixing stress sources. Figure 1 shows the parameters for CW, MW1, and MW2, respectively.

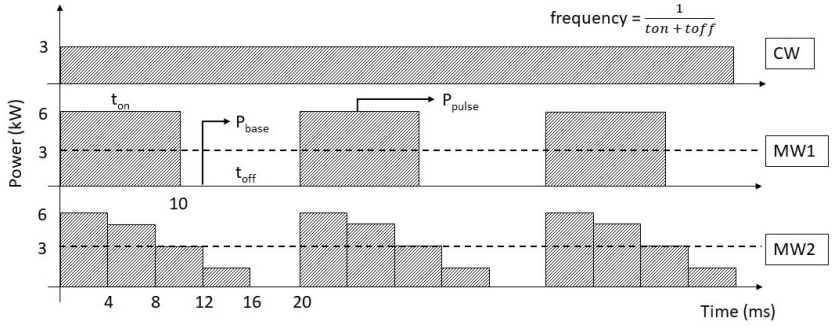

Figure 1. Laser power distribution for CW, MW1, and MW2 tests.

2.2 Porosity Study Parameters

Pulse power was set at 4 kW and base power at 0 kW, giving an average power of 2 kW. To deliver energy intermittently, the laser was turned on (t_{on}) and off (t_{off}) at specific times to give equal time intervals, resulting in a duty cycle of 50%. Modulation frequency varied between 20 Hz and 100 Hz, which combined with the welding speed of 1 m/min, resulting in a range of modulation values similar to Heider *et al.* (2015). These values result in different pulse overlap percentages, chosen to evaluate the pore formation tendency with the increase in frequency. All parameters are shown in Figure 2 and the sample names are related to the frequency applied.

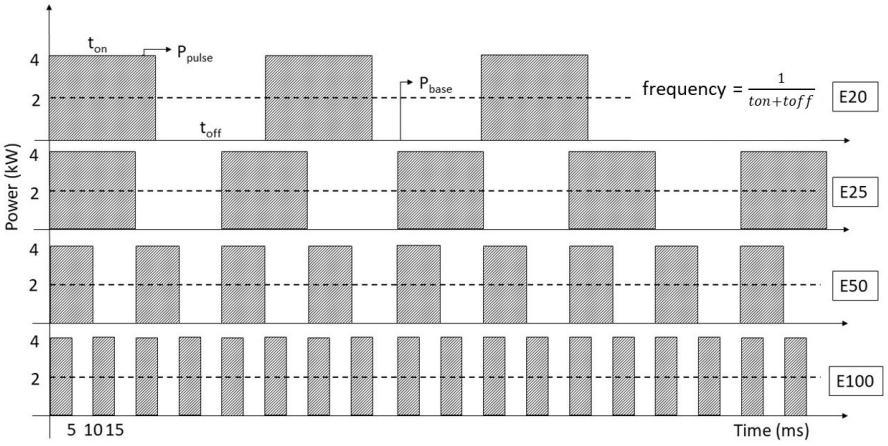

Figure 2. Power distribution considering frequency variation.

Frequency is controlled by pulse time (on) and base time (off). For a duty cycle of 50%, pulse time and base time are the same. Longer pulse and base times result in lower frequency values. Assuming a theoretical diameter of 800 μm for the spot size and a welding speed of 1 m/min, it is possible to determine the pulse overlap obtained for each modulation frequency. Figure 3 shows the pulse overlapping behavior for the E20 (20 Hz) and E100 (100 Hz) tests and Table 1 shows pulse overlap values.

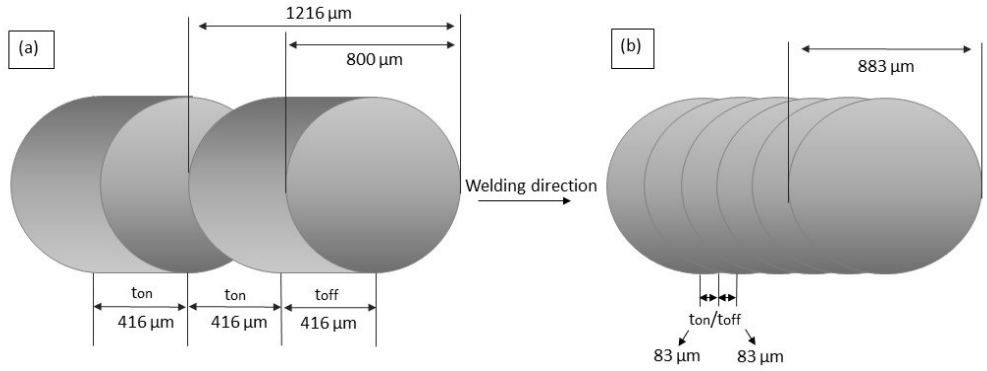

Figure 3. Pulse overlaps for (a) E20 (20 Hz) and (b) E100 (100 Hz) samples.

Table 1. Pulse overlap percentage for each test.

Sample	Laser dislocation during t_{on}/t_{off}	Overlap (%)
E20	0.416 mm	22.2%
E25	0.333 mm	31.7%
E50	0.166 mm	58.3%
E100	0.083 mm	76.6%

In the E20 test, 22.2% of the first pulse is overlapped by the next pulse, while in the E100 test this value reaches 76.6%. This demonstrates that even in the case of relatively large spot size, this difference will influence the waviness at the weld bead bottom.

3. RESULTS

3.1 Residual stresses study

The residual stress results for tests CW, MW1, and MW2 carried out using SAE 4140 steel, in directions parallel to the welding bead, are shown in Figure 4. The magnitude of the residual stress measured with a hole drilled in a region far from the bead is also shown in order to identify the stress states in the base metal. The yield strength of tempered SAE 4140 is 690 MPa (Bruce, 1991) (represented by the dashed lines in the plots).

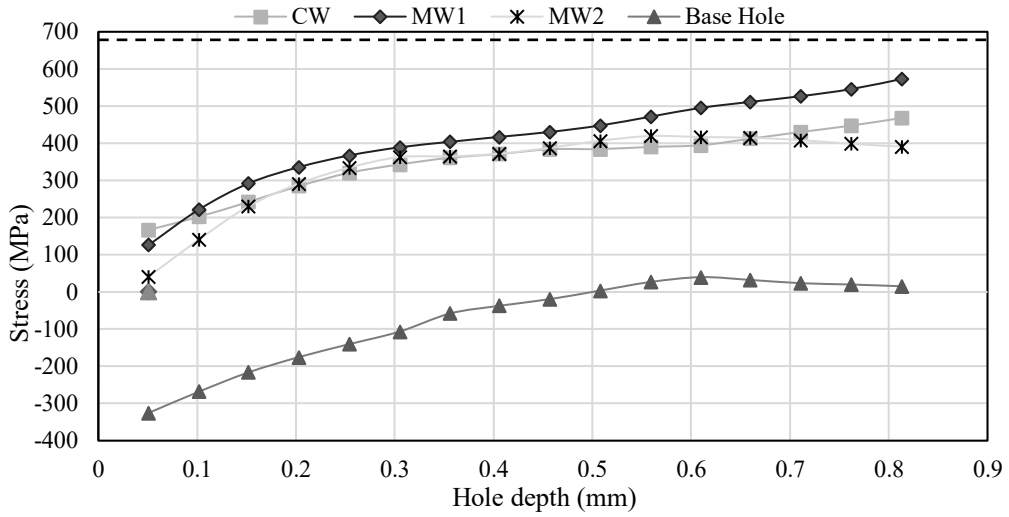

Figure 4. Residual stress values for CW, MW1, MW2, and the base hole in the direction parallel to the welding bead.

Some interesting aspects can be noted in Figure 4. The stress values for the base hole start at -325 MPa, representing compressive forces, probably due to previous machining processes performed during the sample fabrication. When the hole depth increases, the stresses tend toward zero, confirming the absence of residual stress in the base metal core, probably due to stress relief during heat treatments performed before the machining.

Beads CW, MW1, and MW2 showed higher magnitudes of residual stress, in the field of tractive forces, above the values obtained for the base material, confirming the presence of welding-induced phenomena. The high energy density causes thermal cycles, resulting in deep penetration welds. It can be seen that the MW1 test provided the highest residual stress values through the entire hole depth, the difference being accentuated as the hole becomes deeper. At the same time, it can be noted that for tests MW1 and CW the residual stress magnitudes reach values of 82% and 68% respectively to the yield strength of SAE 4140, represented by the dashed line in Figure 4. These magnitudes should be considered carefully as the high-stress levels mean that yielding could occur around the hole. The mathematical model used to compute the stresses released by the hole drilling technique involves the application of elastic principles. Consequently, the residual stresses could be overestimated by the computation model, as also experimentally observed and analyzed by previous works (Beghini, 2010; Nobre, 2018; Vangi, 2010), and the real values could be lower. Nevertheless, the measurements clearly show that the stresses in the last hole increments are tensile and with a considerable magnitude for all of the tests performed in the welded samples. The lowest residual stress values were obtained in MW2 test, the values being 181 MPa lower compared with MW1 and 77 MPa lower compared with CW, for a depth of 0.8 mm.

To observe the microstructure and morphology of the beads and evaluate their correlation with residual stress behavior, the beads were cross-sectioned, ground, and polished. Macrographs were then obtained, as shown in Figure 5.

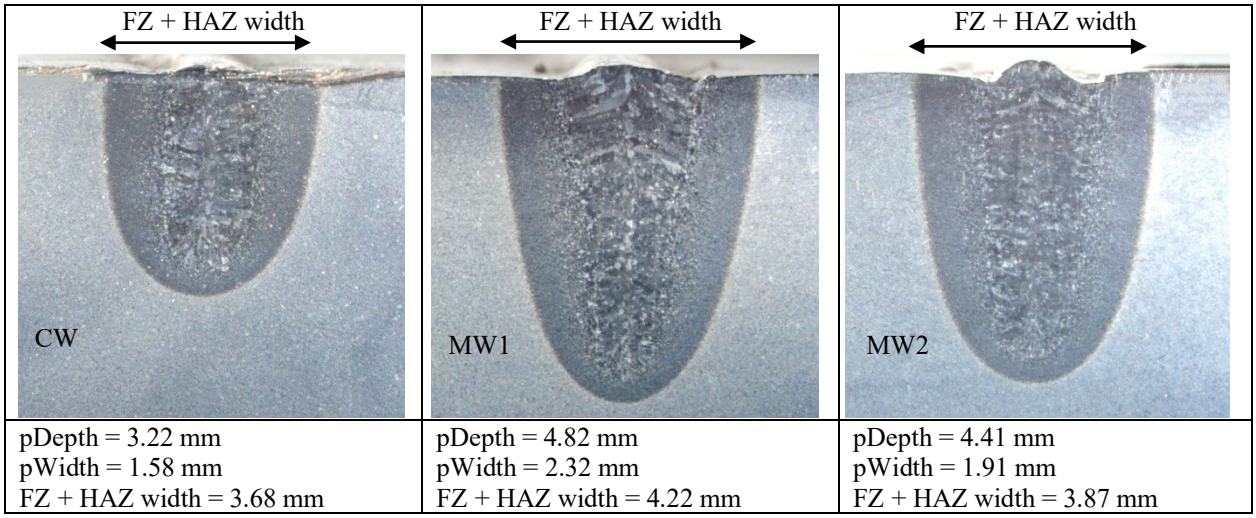

pDepth = 3.22 mm pWidth = 1.58 mm FZ + HAZ width = 3.68 mm	pDepth = 4.82 mm pWidth = 2.32 mm FZ + HAZ width = 4.22 mm	pDepth = 4.41 mm pWidth = 1.91 mm FZ + HAZ width = 3.87 mm

Figure 5. Macrographs of cross-sections of CW, MW1, and MW2 beads, with penetration width, depth, and total width (FZ + HAZ).

The images in Figure 5 show beads with coarse and columnar grains in the region of the fusion zone, which extends to the beginning of the HAZ. SAE 4140 steel is, as previously mentioned, a hardenable steel that is susceptible to martensitic transformation. This displacive transformation occurs due to thermal cycles provided by the welding process. At some stage, the peak temperature surpasses the steel Ac_1 temperature and a lattice expansion of 4.43% occurs during cooling in the transformation area. This introduces stresses since the transformation occurs inside the fusion zone, represented by a small fraction of the total component volume. At the same time, the rapid solidification in laser processes provides conditions that allow the martensite to remain at room temperature. The FZ in both beads showed an as-transformed martensitic structure with columnar grains. This is frequently observed in bead fusion zones as a consequence of growth at 90º in the relation to fusion boundary, in the opposite direction to the maximum heat flow. Different penetration depths and widths are observed since dissimilar power modulation waves generate distinct laser beam-component interactions in different small fractions of time, even though all welding processes were performed at the same welding energy. This can cause different degrees of martensitic transformation, which affects the amount of lattice expansion.

Regarding the different results obtained for the residual stresses in the holes produced at 3 mm from the center of the bead, some explanations can be postulated. The results for the residual stresses in the direction parallel to the bead showed that the MW1 bead produced with the square power modulated emission has the greatest welding induced stresses. The cross-sectional images showed that this weld reached the highest penetration depth (4.82 mm) and also the largest bead width (2.32 mm). This can be attributed to the longer t_{on} time (10 ms) at higher power (6 kW), resulting in a higher amount of energy being supplied in this fraction of time, changing the bead morphology, as also observed by Stritt *et al.* (2010). This results in a greater volume fraction of martensite present in this weld, since the entire FZ transforms, as previously

explained. This greater volume leads to higher internal stresses to accommodate the volumetric expansion of martensite, introducing more tension. Moreover, the greater energy delivered (6 kW) during t_{on} in the test MW1 is instantaneously reduced to zero at base power (t_{off}), which increases the cooling rate between each pulse due to the great power amplitude (the difference between peak and base power) and influences the martensite transformation in HAZ region, as observed by Akman *et al.* (2009).

Regarding morphology, the larger bead width of the test MW1 pushes the HAZ to regions further away from the center of the bead, which brings the drilled hole closer to regions with higher residual stresses, such as HAZ, since the hole is always drilled at the same distance of 3 mm from the center of the bead. This characteristic may also contribute to the greater presence of residual stresses in the case of the modulated wave MW1 compared to the CW, in contrast to the results obtained by Mehdi *et al.* (1998) in comparative research on TIG welding.

It can be noted that, as previously mentioned, the drilled hole, represented by the dashed lines in the figure, is closest to HAZ for the MW1 bead, due to its larger FZ + HAZ width (4.22 mm). In addition, a larger volume of martensite can be assumed as a consequence of a larger fusion zone, which introduces greater variations in volume, contributing to increased stress.

Concerning the CW and MW2 beads, it was noted that with a distance of 3 mm between the bead center and the drilled hole center, bead MW2 presents lower residual stress magnitudes in the parallel direction, even though it has a greater width (1.91 mm) and consequently a greater volume fraction of martensite than the CW bead. This bead was produced under step-shaped power emission, with the power being gradually reduced until its complete extinction, with the last power step of 1.5 kW, resulting in a lower cooling rate compared to the CW and MW1 tests which have, respectively, a constant (3 kW) and a more abrupt power emission intermittency (6 and 0 kW). Also, this test is characterized by a larger pulse overlap leading to rewarming by successive pulses. The reheating can act as a stress-relieving mechanism as observed, for example, for remelting stress relief methods. This relief occurs due to the increased agitation of the atoms in the heated region, which favors the rearrangement and absorption of residual stresses by the component, phenomena which do not occur in the constant power emission. In this regard, even though the FZ + HAZ width was 5% larger, the residual stresses measured at 3 mm from the center of the MW2 bead were, throughout the entire drilling hole increment, lower than those of the bead produced with CW, being 16% lower at 0.8 mm depth. In addition, this weld presented a penetration depth of 37% greater than that of the continuous wave and an aspect ratio value of 11% higher than the bead MW1, showing a greater power efficiency combined with lower residual stresses.

3.2 Porosity study

To assess the pulse overlap, the top surface images shown in Figure 6 were analyzed.

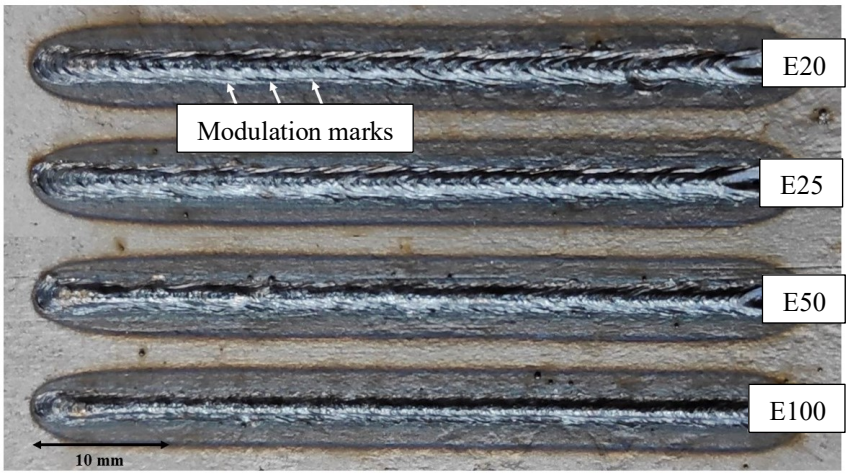

Figure 6. Top weld surface resulting from different modulation frequencies (20 Hz to 100 Hz).

As expected, due to a greater degree of overlap at higher frequencies, it is difficult to distinguish the modulation marks, for example, in sample E100. On the other hand, as observed in Figure 6, in the case of low frequency (E20), the pulse separation can be noted. Due to the longer t_{off} time and the welding speed, the laser moves a greater distance (0.416 mm) before the subsequent t_{on}, in this test. Moreover, the distance between the ending of each pulse is obtained by multiplying the total $t_{on} + t_{off}$ time by the welding speed, resulting in a distance of 0.83 mm.

Regarding weld bead dimensions, the average width of the weld bead was gradually reduced for higher values of modulation frequency while the average bead penetration depth increased and the degree of oscillation decreased, as indicated by the standard deviation bars in Figure 7.

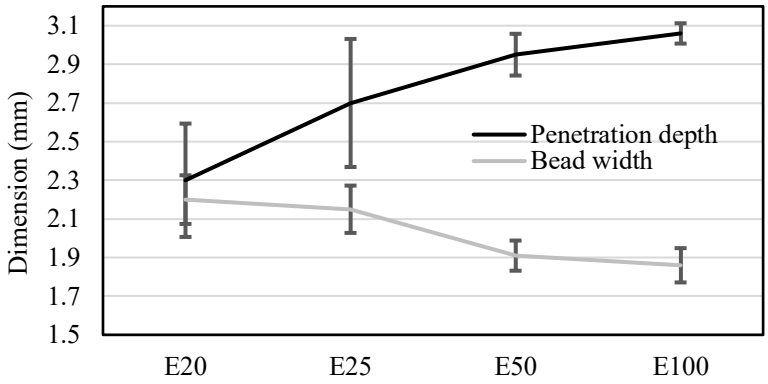

Figure 7. Effect of modulation frequency on bead morphology (bead penetration and width).

Matsunawa *et al.* (1998) and Kaplan (1994) explained the width growth behavior through multiple reflections of the beam on the keyhole walls. As the beam remains on for longer times in tests with lower frequencies, more internal reflections occur, widening the weld bead. A wide bead is important for joints that require low geometrical tolerances and can improve process robustness. The increase in penetration depth can be attributed to better control of keyhole oscillations, which enhances the energy absorption by the cavity and the weld pool, as stated by Shimokusu *et al.* (2003).

In order to visualize the penetration depth oscillations, the samples were cut longitudinally and the results can be seen in Figure 8.

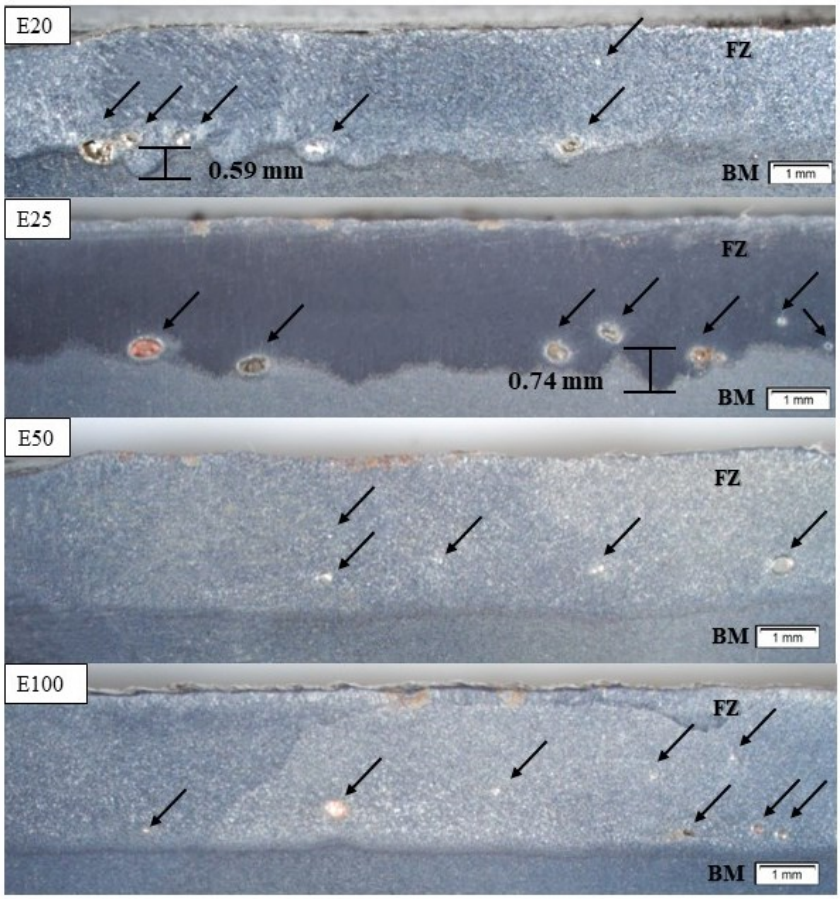

Figure 8. Longitudinal bead cross sections resulting from different modulation frequencies, (E20) average pore area = 0.22 mm², (E25) average pore area = 0.25 mm², (E50) average pore area = 0.1 mm², and (E100) average pore area = 0.06 mm². Pores are indicated by arrows and lines indicate depth variation.

In the longitudinal cross-sections, a higher penetration depth variation was observed for low frequencies (E20 and E25) along with a higher number of pores with different sizes and positions, allowing a qualitative analysis. Figure 9 shows the correlation between penetration depth variation and the average pore area for each frequency.

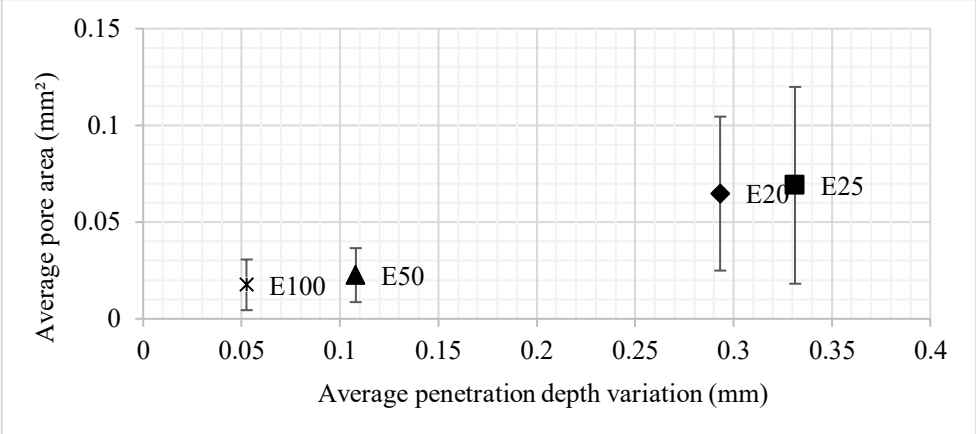

Figure 9. Correlation between average bead depth oscillation and average pore area.

The variation in the penetration depth is a result of the overlap value for each condition, which directly affects the oscillation of the keyhole. The profile discontinuity can impair the final quality of the weld, since the components may not be completely welded and the desired uniform depth may not be achieved, thus reducing the mechanical properties. The effect observed in Figure 9 can be explained through the percentage of overlap between the power pulses and t_{on} times. The tests performed at low modulation frequency showed percentages of pulse overlap in the order of 22.2% to 31.7% (Table 2). Besides, longer pulse times (20 ms and 25 ms) make the keyhole more susceptible to oscillations since the keyhole growth rate reaches a saturation point a few milliseconds after opening, as previously mentioned by Shimokusu *et al.* (2003). Once the keyhole reaches its maximum penetration depth, the forces resulting from the balance between vapor pressure, recoil force, density, and viscosity tend to cause the keyhole to oscillate over time. These oscillations generate variations in the penetration depth and lead to gas and vapor trapping during the welding process.

On analyzing qualitatively, the pores present in the longitudinal sections, it is evident that lower frequencies (20 Hz and 25 Hz) led to larger pores than higher frequencies (50 Hz and 100 Hz). Although pores have not been eliminated, the tendency of reduction in pore size with the increase in modulation frequency is interesting in order to enhance the mechanical properties since the pores act as stress concentrators (Rice, 1993). Furthermore, small pores reduce pore-crack interactions due to the small pore area (Rice, 1997). The pores present in the samples obtained at low frequencies are located at the bottom of the keyhole. This suggests that the pores observed for samples E20 and E25 are the result of vapor gas trapped at the bottom of the molten pool, due to the strong penetration depth oscillations observed in the cross-sections in Figure 9. The laser beam vaporizes the metal inside the cavity and this vapor is trapped through the oscillation and collapsing of the keyhole and cannot escape due to the rapid solidification of the molten pool. In the same way, the smaller pore size for higher frequencies (50 Hz and 100 Hz) can be correlated to the lower degree of depth oscillations, which suggests better control of the keyhole stabilization during welding. Moreover, setting the applied frequency value close to the keyhole self-fluctuation frequency may prevent the formation of pores. Furthermore, the higher percentage of overlap in these tests may have facilitated the floating of bubbles by vibrating and remelting a portion of the molten pool produced by the previous pulse, due to its higher frequency. This remelting could have the same effect as the conventional second welding pass but with a significant cost reduction. It was observed in these tests that the bubbles were found mostly in the middle part of the fusion zone, which suggests they could move toward the surface through the molten pool during welding. This means that power modulation can reduce the porosity with the combination of two main factors: an optimum frequency to avoid keyhole oscillation and an optimized overlap to facilitate bubble floating during welding.

4. CONCLUSIONS

Welding bead-on-plate tests were conducted using continuous and modulated power emission regimes, maintaining the energy level constant. Hole drilling tests and longitudinal cross-sections were performed in order to measure the residual stresses in a region 3 mm from the bead center and to observe porosity formation, respectively. The following conclusions can be drawn from the results obtained:

- Modulated laser power emission can change the bead morphology by delivering energy in different magnitudes and times, which modifies the bead mechanisms of melting, cooling, and solidification in a small fraction of

time, even for processing performed under the same welding energy. Square-shaped power emission produced larger and deeper beads, with larger HAZ and FZ, resulting in higher residual stresses in comparison to continuous and step-shaped waves, at a distance of 3 mm from the bead center.

- Step-shaped laser power modulation can result in lower cooling rates and stress relief during welding due to bead reheating and molten pool agitation caused by the pulse overlap. Moreover, the greater energy distribution in this mode compared to the square-shaped wave means that the bead is exposed to the higher power (6 kW) for shorter exposure times (4 ms). This results in narrower beads, smaller HAZ, smaller fusion zones rich in martensite, and, thus, a lower amount of residual stress.
- Most pores resulting from low modulation frequencies (20 Hz and 25 Hz) had diameters > 100 μm and are located at the bead root. This suggests, as also observed in the previously mentioned studies, that their formation may be due to vapor entrapment resulting from strong keyhole oscillations, observed in the figures and from the measured bead penetration depth oscillations. Combined with a high laser welding speed, this impedes the vapor bubbles from floating to the surface due to rapid solidification. These oscillations may have occurred due to the longer t_{on} times which led to saturation of the keyhole growth and cavity collapse.
- High modulation frequencies (50 Hz and 100 Hz) produced beads with smaller pores, located in intermediate zones of the bead depth. Longitudinal cross-sections showed that these beads presented less penetration depth variation, which suggests a more stable welding process probably due to two main process characteristics: (1) shorter t_{on} times that led to less keyhole growth saturation and collapse, mitigating the first mechanism of pore formation and (2) applied frequencies of 50 Hz and 100 Hz combined with a welding speed of 1 m/min may be closer to the keyhole self-fluctuation frequency. Simultaneously, the higher pulse overlap obtained in these tests may have led to the formation of larger bubbles that float towards the surface partially due to the remelting and vibration of the previously solidified structure. These phenomena may not have occurred for small pores due to their reduced mobility.

5. REFERENCES

Akman, E.; Demir, A.; Canel, T.; Sınmazçelik, T., 2009. “Laser welding of Ti6Al4V titanium alloys”. *J. Mat. Proces. Technol.*, 209(8), 3705–3713. DOI:10.1016/j.jmatprotec.2008.08.026.

Albertazzi A., Viotti M.R., Veiga C., 2016. “A portable optical DSPI system for residual stresses measurement by hole drilling using the integral method in terms of displacement”, Mat. Res. Proc. 2 449–454.

Albertazzi A., Zanini F., Viotti, M.R., Veiga, C.L.N., 2015. “Residual stresses measurement by the hole-drilling technique and DSPI using the integral method with displacement coefficients”, in: 5th International Symposium on Experimental Mechanics e 9th Symposium on Optics in Industry, 2015, v. 1. p. 1–7.

Beghini, M.; Bertini, L.; Santus, C. 2010. “A procedure for evaluating high residual stresses using the blind hole drilling method, including the effect of plasticity”. *J. Strain Anal. Eng. Des.*, 45(4), 301–318. DOI:10.1243/03093247jsa579.

Bruce A. Becherer and Thomas J. Witheford, 1991. “Heat Treating of Ultrahigh-Strength Steels, Heat Treatment”. *ASM handbook*. Vol. 4. ASM Handbooks Online. Materials Park, OH, ASM International.

Cavilha Neto, F.; Fredel, M. C.; Pereira, M., 2020. “Laser Power Modulation To Grain Refinement of SAE 1045 Steel”. *J. Laser Appl.*, *022027*, 1–7.

Cavilha Neto, F.; Pereira, M.; Paes, L.E.S.; Fredel, M.; Bossa, L.F., 2021. “Effect of power modulation frequency on porosity formation in laser welding of SAE 1020 steels”. *Int. J. Adv. Manuf. Tech*nol. 112, 2509–2517.

Deng, D.; Murakawa, H. 2006. “Prediction of Welding Residual Stress in Multi-Pass Butt-Welded Modified 9Cr-1Mo Steel Pipe Considering Phase Transformation Effects”. Comput. Mater. Sci., 37 (3), 209–219.

Derakhshan, E. D.; Yazdian, N.; Craft, B.; Smith, S.; Kovacevic, R., 2018. “Numerical Simulation and Experimental Validation of Residual Stress and Welding Distortion Induced by Laser-Based Welding Processes of Thin Structural Steel Plates in Butt Joint Configuration”. *Opt. Laser Technol*., 2018, 104, 170–182.

Heider A., Weber R., Herrmann D., Herzog P., Graf T., 2015. “Power modulation to stabilize laser welding of copper”. J. Laser Appl. 27(2), 022003–.

Huang L., Hua X., Wu D., Li F., 2018. “Numerical Study of Keyhole Instability and Porosity Formation Mechanism in Laser Welding of Aluminum Alloy and Steel”. J. Mater. Processing Technol. 252, 421–431.

Huang, H.; Wang, J.; Li, L.; Ma, N. 2016. “Prediction of Laser Welding Induced Deformation in Thin Sheets by Efficient Numerical Modeling”. *J. Mater. Process. Technol.*, *227*, 117–128.

Jiang M., Chen X., Chen Y., Tao W., 2019. “Increasing Keyhole Stability of Fiber Laser Welding under Reduced Ambient Pressure”. J. Mater. Processing Technol. 268, 213–222.

Junaid, M.; Khan, F. N.; Rahman, K.; Baig, M. N., 2017. “Effect of laser welding process on the microstructure, mechanical properties and residual stresses in Ti-5Al-2.5Sn alloy”, *Opt. Laser Technol.* 97, 405-419.

Kaplan A., 1994. “A Model of Deep Penetration Laser Welding Based on Calculation of the Keyhole Profile”. J. Phys. D: Applied Phys. 27 (9), 1805–1814.

Kim, S. H.; Kim, J. B.; Lee, W. J., 2009. "Numerical Prediction and Neutron Diffraction Measurement of the Residual Stresses for a Modified 9Cr-1Mo Steel Weld". J. Mater. Process. Technol., 209 (8), 3905–3913.

Kouraytem N., Li X., Cunningham R., Zhao C., Parab N., Sun T., Rollett A.D., Spear A.D., Tan W., 2019. "Effect of Laser-Matter Interaction on Molten Pool Flow and Keyhole Dynamics". Physical Review Applied. 11 (6), 1.

Lei, Z.; Zou, J.; Wang, D.; Guo, Z.; Bai, R.; Jiang, H.; Yan, C., 2020. "Finite-Element Inverse Analysis of Residual Stress for Laser Welding Based on a Contour Method". *Opt. Laser Technol.*, 129, 106289.

Liang, R.; Luo, Y.; Li, Z., 2018. "The Effect of Humping on Residual Stress and Distortion in High-Speed Laser Welding Using Coupled CFD-FEM Model". *Opt. Laser Technol.*, 104, 201–205.

Lin R., Wang H.P., Lu F., Solomon J., Carlson, B.E., 2017. "Numerical Study of Keyhole Dynamics and Keyhole-Induced Porosity Formation in Remote Laser Welding of Al Alloys". Int. J. Heat Mass Transf. 108, 244–256.

Matsunawa, A.; Kim, J.-D.; Seto, N.; Mizutani, M.; Katayama, S., 1998. "Dynamics of Keyhole and Molten Pool in Laser Welding". *J. Laser Appl.*, *10* (6), 247–254.

Mehdi, B.; Badji, R.; Ji, V.; Allili, B.; Bradai, D.; Deschaux-beaume, F.; Soulié, F., 2016. "Microstructure and Residual Stresses in Ti-6Al-4V Alloy Pulsed and Unpulsed TIG Welds". J. Mater. Process. Technol., 231, 441–448.

Nobre, J.P.; Kornmeier M.; Scholtes, B., 2018 "Plasticity Effects in the Hole-Drilling Residual Stress Measurement in Peened Surfaces". *Exp. Mech.,* 58, 369–380.

Paddea, S.; Francis, J. A.; Paradowska, A. M.; Bouchard, P. J.; Shibli, I. A., 2012. "Residual Stress Distributions in a P91 Steel-Pipe Girth Weld before and after Post Weld Heat Treatment". Mater. Sci. Eng. A, 534, 663–672.

Papadopulos, F.; Spinelli, M.; Valente, S.; Foroni, L.; Orrico, C.; Alviano, F.; Pasquinelli, G., 2007. "Common Tasks in Microscopic and Ultrastructural Image Analysis Using ImageJ". *Ultrastructural Pathology*, 31 (6), 401–407.

Rice, R.W., 1993. "Comparison of stress concentration versus minimum solid area based mechanical property-porosity relations". J. Mat. Sci. , 28(8), 2187–2190.

Rice, R.W., 1997. "Limitations of pore-stress concentrations on the mechanical properties of porous materials". J. Mat. Sci. 32(17), 4731–4736.

Santos Paes, L. E.; Pereira, M.; Weingaertner, W. L.; Scotti, A.; Souza, T., 2019. "Comparison of Methods to Correlate Input Parameters with Depth of Penetration in LASER Welding". *Int. J. Adv. Manuf. Technol.*, *101* (5–8), 1157–1169.

Schaefer, M.; Kessler, S.; Scheible, P.; Graf, T., 2017. "Modulation of the Laser Power to Prevent Hot Cracking during Laser Welding of Tempered Steel". *J. Laser Appl.*, *29* (4), 042008.

Shimokusu Y., Fukumoto S., Nayama M., Ishide T., Tsubota S., Matsunawa A., Katayama S., 2003. "Application of Pulse-Modulated High-Power YAG Laser to Welding of Heavy Plates". Welding Int. 17 (7), 534–540.

Stritt, P.; Weber, R.; Graf, T.; Müller, S.; Ebert, C., 2010. "Laser Power Modulation at the Threshold from Heat-Conduction to Deep-Penetration Welding". *29th International Congress on Appl. of Lasers and Electro-Opt., ICALEO 2010 - Congress Proceedings*, *103*, 217–224.

Tamma, K. K.; Zhou, X.; Anderson, C. V. D. R., 2014. *Encycl. Therm. Stresses*.

Tsukamoto, S.; Kawaguchi, I.; Arakane, G.; Honda, H., 2003. "Keyhole Behavior in High Power Laser Welding". *First Int. Symp. High-Power Laser Macroprocessing*, *4831*, 251.

Vangi, D.; Tellini, S. Hole-Drilling Strain-Gauge Method: "Residual Stress Measurement With Plasticity Effects". *J. Eng. Mat. Technol.*, 2010, 132(1), 011003.

Viotti, M.R., Albertazzi, A. 2013. "Compact sensor combining digital speckle pattern interferometry and the hole-drilling technique to measure nonuniform residual stress fields", Opt. Eng. 52 (10), 101905.

Zhang L.J., Liu J.Z., Pei J.Y., Ning J., Zhang L.L., Long J., Zhang G.F., Zhang J.X., Na S.J., 2019. "Effects of Power Modulation, Multipass Remelting and Zr Addition Upon Porosity Defects in Laser Seal Welding of End Plug to Thin-Walled Molybdenum Alloy". J. Manuf. Processes, 41, 197–207.

Zhang Y., Lin Q., Yin X., Li S., Deng J., 2018. "Experimental Research on the Dynamic Behaviors of the Keyhole and Molten Pool in Laser Deep-Penetration". J. Phys. D: Applied Phys. 51 (14), 145602.

6. RESPONSIBILITY NOTICE

The authors are the only responsible for the printed material included in this paper.